Error Propagation Concepts Including Flight Dynamics for Total System Performance Analysis During GBAS based Initial CAT-III Approach and Landing

Thomas Dautermann*, Boubeker Belabbas and Michael Meurer
German Aerospace Center (DLR)
Institute of Communication and Navigation
82234 Wessling, Germany
* *Thomas.Dautermann@dlr.de*

ABSTRACT

In order to assess the integrity risk for GBAS based automatic approach and landing, we investigated a total performance concept of a combined system consisting of an ILS look-a-like GBAS landing system (GLS) and a DeHavilland Dash-2 Beaver aircraft. We propagated four basic pseudorange errors to a position error distribution, which was then the source of position uncertainties for the GLS installed in the aircraft. Results show that the vertical total system error (TSE) in the steady state final approach lags behind the vertical navigation system error (NSE). The TSE is smoothed and preserves the general temporal sequence of the error. A reduction of 30% of the TSE standard deviation with respect to the NSE only occurs during a period of glide slope overshoot, where the autopilot uses large and steadily declining elevator deflections to return to the desired glide path. With minor adaptations this concept can be refined and a possible error reduction may be achieved.

1 INTRODUCTION

In a differential GPS system such as the ground based augmentation system (GBAS) for precision approaches of aircraft, GPS reference stations with known locations are utilized to determine and remove most of the ranging uncertainties of the GNSS system in use. Corrections are broadcast to the aircraft and all but spatially decorrelated errors are eliminated. These residual pseudorange errors lead to a position uncertainty of the aircraft.

To qualify for category I (CAT-I) precision guidance, the system has to guarantee that undetected pseudorange errors do not cause horizontal and vertical position errors larger than horizontal and vertical alert limits with an integrity risk smaller than 2×10^{-7} per approach, for category III (CAT-III) with a probability smaller than 10^{-9} per 15 s (EUROCAE ED-144, 2007; RTCA DO-245A, 2004). In order to reach the low integrity risk threshold for CAT-III using a single frequency single constellation, a current concept actively pursued by the research community is the integrity assessment of a joint navigation and flight dynamics and control system of the aircraft.

Here, we study the errors of a single frequency GNSS navigation system and propagate those errors through the navigation solution to the position domain. On this level they interlock with the flight dynamics equations (FDE), a set of twelve ordinary differential equations which can be solved using standard Runge-Kutta Methods as presented, for example, by Gear (1991) or Dormand and Prince (1980).

2 GBAS ERRORS

As described in detail by Dautermann et al. (2009), we combined the probability density functions (PDFs) for the four individual error sources multipath, differential troposphere, differential ionosphere and receiver noise to a single, carrier smoothed pseudorange PDF.

For the multipath PDF we followed Pervan et al. (2000) and assumed a uniformly distributed phase shift between reflected and original carrier phase. This leads to the following expression for the distribution of the multipath error (for details

see Pervan et al., 2000)

$$p_{mp}(\epsilon) = \frac{1}{b^2 \sin\phi} \ln\Big[\frac{1+\sqrt{1-(\frac{(\epsilon - a\sin\phi)}{b\sin\phi})^2}}{\frac{|\epsilon - a\sin\phi|}{b\sin\phi}}\Big] \tag{1}$$

where b is the maximum amplitude of the reflected with respect to the original signal, ϕ the elevation angle and a the variable bias of the distribution. For our theoretical example we choose the receiver to have an ultra-narrow correlator spacing and a maximum multipath of 3 m as depicted by the multipath envelope in Novatel (2002). This value will, however, never be reached, since the PDF truncates at a smaller value. Since multipath may, in general, be biased (Braasch, 1992) we used a symmetry offset from the ordinate of $a = 0.5\ m$ in the work presented here. The ionosphere gradient distribution has exponential character as shown by Christie et al. (1999) and more recently confirmed by Mayer et al. (2008). For this work, we extracted the exponential distribution for the ionosphere gradient PDF from the afore mentioned publication.

$$p_{ivg}(y) = \frac{ln(10)}{26} 10^{-\frac{|y|}{13}}; \tag{2}$$

where y is the ionospheric gradient in ppm or mm/km. To translate this gradient PDF into a pseudorange error distribution, we assume a worst case user position at the edge of the GBAS service volume of 20 nm (35.04 km). For the residual tropospheric error caused by the location difference between aircraft and GBAS ground station, we utilized the model adopted by the Radio Technical Commission for Aeronautics (RTCA, DO245A (2004), Section 3.3.2.14) for the local area augmentation system. As input parameters, we chose an airplane altitude of 4000ft (1219.2 m) and a relative humidity of 100%. Lastly, we used receiver noise specifications of the Novatel OEMV-1 positioning engine. These errors are mainly due to thermal and code noise and follow a zero mean Gaussian with a standard deviation of $\sigma_{N_0} = 0.04\ m$ (Novatel Datasheets).

The GBAS ground subsystem employs a 100s carrier-phase smoothing filter (Hatch filter) as defined in the ED-114 GBAS MOPS (2003) or RTCA DO 245A. For each integer elevation angle, we joined the individual error distributions and conducted a Monte Carlo simulation of the smoothing process using 10^9 samples, equivalent to 15.9 years of data recorded at 2 Hz. The carrier

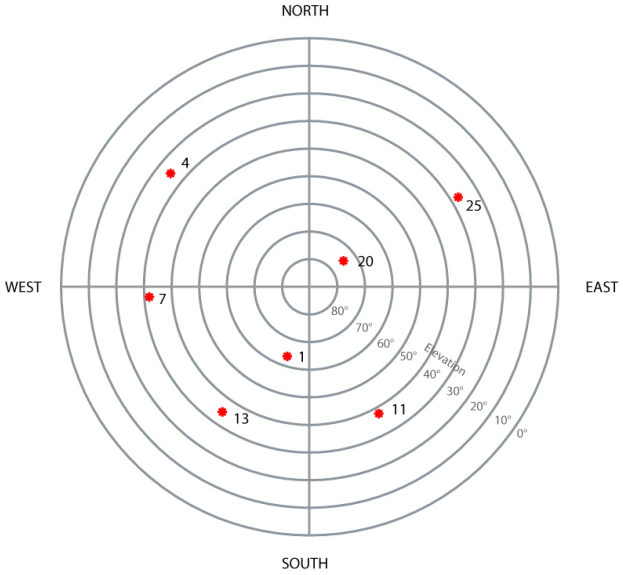

Figure 1 Worst Case Geometry at EDMO which gives a VDOP of 4.32

phase error was assumed to be random Gaussian with $\sigma = 0.02\ m$.

Next, we mapped the error distributions into the position domain using a worst case geometry observed at Oberpfaffenhofen airport (ICAO Identifier EDMO), depicted in Figure 1. Since the GPS constellation approximately repeats at the same location every 24 hours we performed a geometry screening for that period and selected the constellation with the largest vertical dilution of precision (VDoP). This occurred at 12:45 UT with $n = 7$ satellites in view and a VDoP of 4.32. The mapping from pseudorange error $\epsilon_{\hat{\rho}}$ to the position domain error ϵ_x was performed using

$$\epsilon_x = (G^T W G)^{-1} G^T W \epsilon_{\hat{\rho}} \tag{3}$$

with the geometry matrix G (values given in the appendix) in the east-north-up coordinate system and weighting matrix W which contained the sine of the elevation angle (i.e $W_{ii} = \sin\phi_i$)) The error distributions for the east, north and up position components are shown in Figure 2 on a semilogarithmic scale. As expected the Up component PDF is much wider that the one for East or North due to the satellite geometry. North and East component distributions are not equal, but their difference is much smaller compared to the difference between each horizontal and the vertical PDF. Through the process described by equation (3) and the subsequent convolutions, the initial bias originating from the multipath distribution (equation. 1) has been transfered to the re-

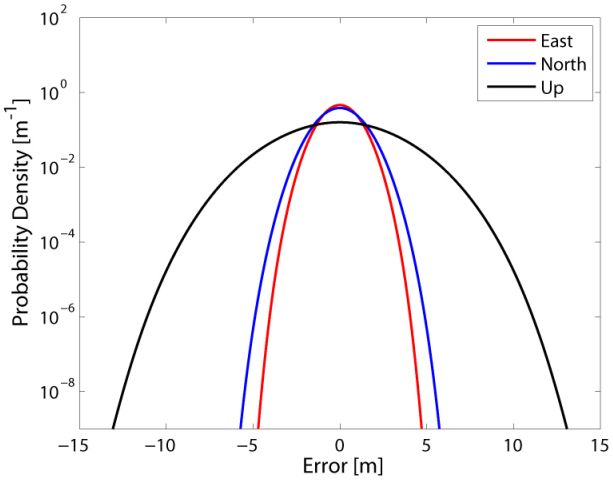

Figure 2 Position Domain Distributions

ceiver clock bias and thus diminished the position PDF offset to a value smaller than our working precision of 1 mm. The PDFs appear Gaussian as a result of the central limit theorem, which states that a sufficient sum of random variables with finite mean and variance will always be normally distributed. Indeed, a best fit with a Gaussian yields all zero means and negligible residuals. The fitted standard deviations are shown in Table 1. The PDFs are quite insensitive to changes in

Component	σ [m]	RMSE
East	0.863	0.00023
North	1.035	0.00019
Up	2.056	0.00016

Table 1 Best Fit Values for the Position Error Distribution

distance of the airplane from the GBAS ground facility, as distributions for ionosphere and troposphere are narrow. With a distance of zero, the fitted east, north and up standard deviations are 0.8455 m, 1.014 m and 2.045 m, respectively. Since these deviations are relatively small and in order not to complicate the calculations unneccesarily, we assumed the position domain error distribution to be constant for the remainder of the analysis.

3 TOTAL SYSTEM CONCEPT

The GLS acts as navigation sensor to provide information about the location of an aircraft flying inside the GBAS service volume. For aviation applications, this location information alone is not sufficient. The navigation system must provide information on how trustful is the given position (integrity), how robust this information is (continuity) and finally how accurate it is (accuracy). The metric used to determine these performances is the navigation system error (NSE). This metric is important to validate the navigation system to be used for different phases of flight. However, for CAT III precision approaches based on GBAS, there is no commitment on the navigation system requirements. Additionally, ILS CAT III requirements are too stringent for a single frequency based GBAS system.

In order to overcome this problem without loosing safety, one can transfer the level of validation from the navigation system to total system (GBAS plus flight dynamics and control), for which requirements as defined in the JAA certification standards - all weather operations (JAA CS-AWO, 2003) must be fulfilled. At this level, GBAS is considered as an erroneous subcomponent and the metric to be used is the Total System Error (TSE), which is composed of NSE and flight technical error (FTE). The total system performance concept consists of assessing the performance parameters (accuracy, integrity, continuity and availability) of the total system with respect to the TSE metric.

4 FLIGHT DYNAMICS MODEL

The dynamics of the airplane is driven by 12 ordinary differential equations derived from the fundamental equations of forces and moments (for a derivation see, for example Rauw (1993) or Stevens and Lewis (1992)). The system of flight dynamics equations can be written in the following form:

$$\dot{\mathbf{x}} = f_1\left(\mathbf{x}(t), \mathbf{u}(t), \mathbf{v}(t), t\right) + f_2\left(\dot{\mathbf{x}}(t), t\right) \qquad (4)$$

where $\mathbf{u}$ is a vector of external control inputs, $\mathbf{v}$ is a vector of external disturbances, $\mathbf{x} = [V\ \alpha\ \beta\ p\ q\ r\ \psi\ \theta\ \varphi\ x_e\ y_e\ H]$ the state vector consisting of true airspeed V, angle of attack α, side slip angle β, the angular velocities p, q, r, roll φ, pitch θ and yaw ψ and x_e y_e H the position of the center of gravity of the aircraft. Since f_1 and f_2 are non-linear functions, the whole system of equations cannot be solved analytically.

The solution of the flight dynamic equations given initial conditions and initial input vectors without feedback from control inputs is called the open loop problem. In a simulation of an automatically controlled aircraft, the trajectory solu-

tion of the flight dynamic equations and comparison with a reference trajectory will determine the control commands needed to steer the aircraft. Here, these control commands are fed back into the flight dynamic equations. This is the closed loop mode.

We used the non-proprietary and complete Simulik model of the DeHavilland Dash-2 Beaver aircraft including autopilot developed by Marc Rauw (1993). The model consists of a flight dynamics module, which contains the FDEs, autopilot and radio navigation blocks which are linked to form the aforementioned closed loop system.

5 SIMULATION

We eliminated the original instrument landing system (ILS) block from the model by Rauw (1993) and created an ILS look-a-like, GNSS Landing System block. Exactly like the ILS this model generates angular deviations from a centerline and a glideslope. To obtain these deviation angles, we used the runway threshold position, runway direction and a three degree glideslope to define a GLS reference point in 30 nm (55.56 km) distance from the threshold, where the localizer and glideslope intersect. Based on this reference point the GLS module computes the two angular deviations and their temporal derivatives, which are fed into the autopilot. Since the GBAS position errors were assumed to not change during the approach, this design generates larger angular deviations as the plane approaches the runway. The GLS module only outputs a new angular deviation every 0.5 s, consistent with the design specifications in the standardization documents EUROCAE ED-144 (2007) and RTCA DO-245A (2004).

To quantify the performance of the system consisting of Dash-2 and GLS, we performed 1000 simulated approaches from an altitude of 4000 ft (1219.2 m) and a distance of 23.8 km from the runway threshold. The approach course was 90^o with the runway oriented in east-west direction. With this geometry our coordinate system matches the East-North-Up system which was used to derive the PDFs for the GBAS position uncertainty. The initial conditions of the system were diluted by adding a random number to each coordinate according to the position domain distributions derived in section 2 (graphically shown in Figure 2). The approach speed was set 87.47 kts (45 m/s).All approaches

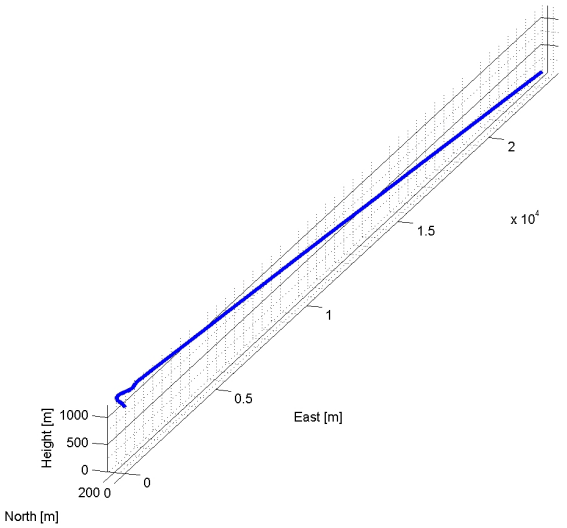

Figure 3 The approach: After the intercept, the Beaver is well established on the glide path

were performed in no-wind conditions and no changes in manifold pressure or engine rpm were allowed. The solver used in Simulink to integrate the FDEs was a fourth order variable step Runge-Kutta algorithm (Matlab implementation ODE45, Dormand and Prince, 1980). An example of a resulting approach trajectory is shown in Figure 3. The airplane starts at a 30^o intercept angle with the autopilot in approach arm mode. Then, as the localizer centers, the asymmetrical autopilot starts to track the approach course. Next, as the glideslope deviation diminishes, the symmetrical component of the autpilot starts to track the glide slope. Now the autopilot has changed its mode from arm to approach and the GLS is being tracked. This switching occurs within the first 50 s of each simulated approach. A sample glide slope interception trajectory (vertical component) is shown in Figure 4 in comparison to the desired altitude. Ideally the aircraft flies straight and level, until it is precisely on the glide path, which it the tracks all the way to the round-out. The Beaver autopilot is constructed such that it overshoots the glide slope and then re-intercepts from above. This is a desired characteristic, since safety is guaranteed above the glide path.

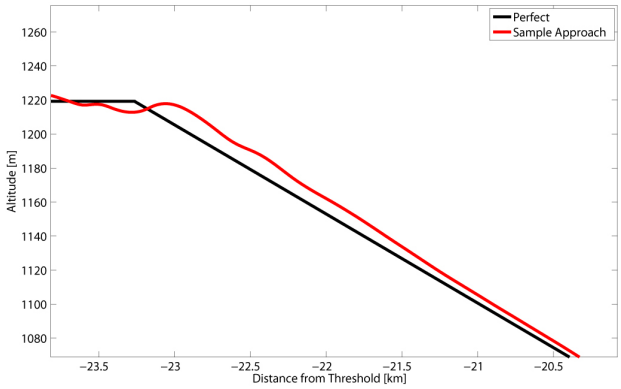

Figure 4 The vertical component of ideal reference trajectory (black) and an example of the vertical Beaver Approach Performance (red)

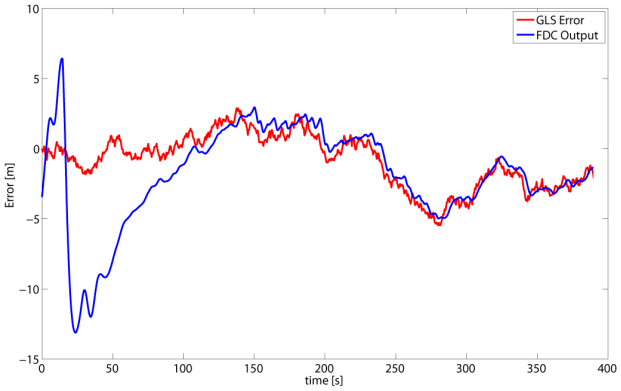

Figure 5 The Beaver position error w.r.to the perfect glide path (TSE, blue) in contrast to the GBAS Position error (NSE, red). A positive error corresponds to a deviation below the reference glide path.

6 RESULTS

Figure 5 shows the difference between the sample and ideal vertical components shown in Figure 4 in comparison to the vertical navigation system error (NSE) of the GLS, which was used to compute the angular deviation from the glideslope. The difference constitutes the above-mentioned TSE.

We can distinguish three separate phases of flight from this graph. First, during the intercept up to 50s, the position error is independent and much larger than the NSE. Then, from 50s up to 110s as the autopilot couples to the GLS, the error begins to approach the one of the navigation system. After 110 s, the position difference of the aircraft from the reference glideslope (total system error or TSE) is closely correlated to the vertical NSE. The TSE is similar in shape to the NSE, but lags 2.95 s behind (peak cross correlation). Moreover, the TSE is visibly much smoother than the TSE. It is notable that the TSE in Figure 5 is not generally smaller than the NSE, from inspection during 50% of the third phase, the TSE is bigger than the NSE.

To quantify this further, we binned the TSE results from all approaches by distance from the threshold and magnitude of the TSE. The result is shown in Figure 6 with a distance bin size of $\Delta x = 0.2382\ km$ and $\Delta TSE = 0.3171\ m$.

As expected, before the autopilot engages, the position error increases in mean and standard deviation over the first bins until 23.1 km distance from the threshold, until the glide slope intercept begins. At all times the airplane overshoots the glideslope and the autopilot corrects the motion with elevator deflections back to the

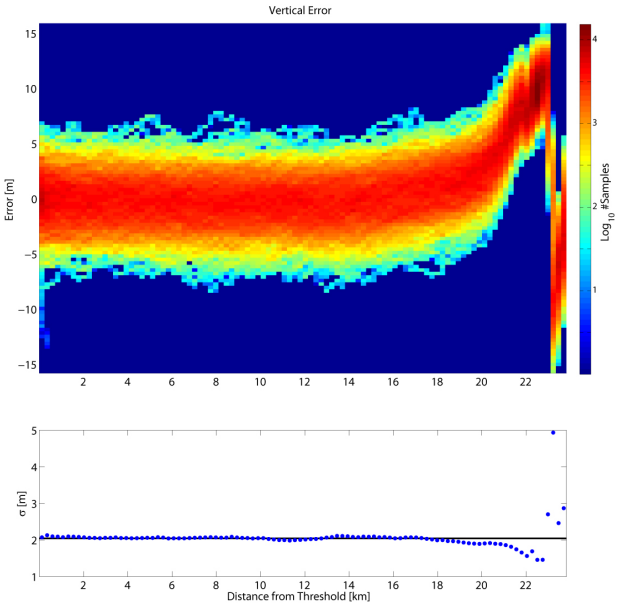

Figure 6 (top) Distogramm (2D Histogram binned by Distance) of the airplane position error. (bottom) Standard deviation per distance bin (blue dots); vertical NSE input standard deviation (black line).

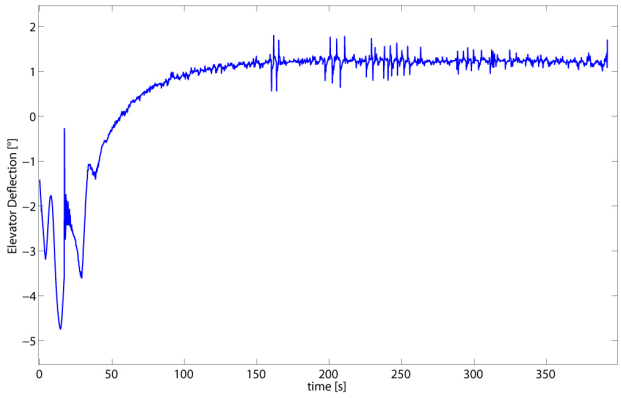

Figure 7 Example of elevator deflection during an approach.

desired path. During this second phase, we observe a narrower TSE distribution, the minimum standard deviation of the bins from 18.8 km to 22.6 km is 1.46 m, a reduction by 30%. In the course of this period the autopilot gives a large, but steadily decreasing elevator command (Figure 7), which effectively narrows the TSE distribution. As the airplane returns to the glidepath and elevator commands diminish in magnitude, the TSE grows again and reaches the input NSE. From here on, the previously mentioned phase 3 begins and the TSE follows the NSE closely.

7 DISCUSSION

We studied the TSE output of a closed loop aircraft model, with respect to a realistic input NSE during the approach phase. During the final approach phase, when the airplane was established on the glide path, we could not discern an error reduction. Only when the elevator was commanded with strong deflection to return to the glideslope, we observed a significant narrowing of the TSE. As the aiplane position approaches the desired glide path, the control surface commands issued by the autopilot diminish and the error reduction effectiveness of the system is reduced. To correct this for future trials, the approach path could be divided into several small segments for increased sensitivity and corrective action, as observed by the initial overshoot. Moreover, the DeHavilland Dash-2 Beaver is an aged airplane (build from 1957-1965) and the autopilot in this model is very crude in its functionality. It is anticipated that with a modern flight director, much better results could be achieved. These modern systems have optimized intercept and tracking functionality limited only by maximum allowed actuator stress and control surface deflections.

Notwithstanding the missing error reduction during the final approach segment, we have shown here that based on the characteristics of autopilot and airplane dynamics, an improvement through the total system concept is in principle possible. This shows promise for the GBAS L1 CAT-III concept (single frequency GBAS CAT-III landings) where the integrity requirements exceed the ones currently possible with CAT-I systems. Here, the total system performance concept could enable certain aircraft to use CAT-I GBAS installation to perform automatic landings according to CAT-III. However, an individual evaluation for each aircraft type/ flight director combination will be necessary to ensure that the integrity requirements can be met. Continuity and availability of such a system would be the same as for CAT-I. For the certification, the influence of singular position error spikes, steps and ramps on the total system performance need to be investigated and the feasibility under those condition needs to be assessed. Here, we expect to see mitigating effects due to the high inertia of the aircraft.

BIOGRAPHY

Thomas Dautermann received his Vordiplom in Physics from the Technical University of Kaiserslautern in 2003. In 2004 he obtained a Master of Science degree in Physics from Purdue University, West Lafayette, IN, USA , followed by a PhD titled "Ionospheric Total Electron Content Perturbations Induced by Lithosphere-Atmosphere-Ionosphere Interaction", also from Purdue University. Thomas Dautermann also holds a commercial pilot certificate with instrument privileges. He is the DLR manager for the German national project HETEREX , which deals with GBAS L1 CAT-III automatic landings and a expert in error propagation and integrity assessments.

Boubeker Belabbas is a research fellow at the DLR (German Aerospace Center) at the Institute of Communications and Navigation at Oberpfaffenhofen near Munich. He is a PhD student at ENPC (Ecole Nationale des Ponts et Chaussées) Paris. He received his MSc degree in Mechanics and Energetic from the Ecole Nationale Supérieure d' Electricité et de Mécanique at Nancy (France) in 1995 and a specialised Mastère in Aerospace Mechanics at the Ecole

Nationale Supérieure de l'Aéronautique et de l'Espace at Toulouse (France) in 2001. His field of work is the integrity of GNSS with its augmentations and its applicability for Safety of Life receivers.

Michael Meurer received the diploma in Electrical Engineering and the Ph.D. degree from the University of Kaiserslautern, Germany. After graduation, he joined the Research Group for Radio Communications at the Technical University of Kaiserslautern, Germany, as a senior key researcher, where he was involved in various international and national projects in the field of communications and navigation both as project coordinator and as technical contributor. From 2003 till 2005, Dr. Meurer was active as a senior lecturer. Since 2005 he has been an Associate Professor (PD) at the same university. Additionally, since 2006 Dr. Meurer is with the German Aerospace Centre (DLR), Institute for Communications and Navigation, where he is the director of the Department of Navigation.

A APPENDIX

Geometry Matrix for the constellation shown in Figure 1:

$$G = \begin{pmatrix} -0.1339 & -0.4250 & 0.8952 & -1.0000 \\ -0.7007 & 0.5720 & 0.4263 & -1.0000 \\ -0.8464 & -0.0549 & 0.5297 & -1.0000 \\ 0.3810 & -0.6946 & 0.6102 & -1.0000 \\ -0.4678 & -0.6744 & 0.5713 & -1.0000 \\ 0.2143 & 0.1610 & 0.9634 & -1.0000 \\ 0.7630 & 0.4580 & 0.4562 & -1.0000 \end{pmatrix} \quad (5)$$

REFERENCES

[1] M. S. Braasch. Characterization of gps multipath errors in the final approach environment. In *Proceedings of the 5th International Technical Meeting of the Satellite Division of the Institute of Navigation*, pages 383 – 394, Albuquerque, NM, 1992.

[2] Jock R. I. Christie, Ping-Ya Ko, Andrew Hansen, Donghai Dai, Samuel Pullen, Boris S. Pervan, and Bradford W. Parkinson. The Effects of Local Ionospheric Decorrelation on LAAS: Theory and Experimental Results. In *ION NTM*, 1999.

[3] Thomas Dautermann, Boubeker Belabbas, and Patrick Remi. A novel integrity concept for gbas precision approaches induced by error propagation with non-gaussian distributions. In *Proceedings of the European Navigation Conference*, May 2009.

[4] J. R. Dormand and P. J. Prince. "A Family of Embedded Runge-Kutta Formulae". *J. Comp. Appl. Math.*, 6:19–26, 1980.

[5] EASA. Certification specifications for all-weather operations (cs-awo), October 2003.

[6] EUROCAE. ED-114: Minimum Operational Performance Specification for Global Navigation Satellite Ground Based Augmentation System Ground Equipment towards Support Category I Operations. Technical report, EUROCAE, 2003.

[7] C.W. Gear. *Numerical Initial Value Problem in Ordinary Differential Equation*. Prentice Hall, Eaglewood Cliffs, New Jersey, 1991.

[8] C. Mayer, N. Jakowski, C. Borries, T. Pannowitsch, and B. Belabbas. Extreme Ionospheric Conditions over Europe observed during the last Solar Cycle. In *Navitec*, number S08-01. European Space Agency, 2008.

[9] Novatel. *Local Area Augmentation System (LAAS) Ground Facility (LGF4) Reference Receiver*. Novatel, "om-20000070" edition, 12 2002.

[10] Boris Pervan, Sam Pullen, and Irfan Sayim. Sigma Estimation, Inflation, and Monitoring In the LAAS Ground System. In *Proceedings of the ION GPS*. Institute of Navigation, 2000.

[11] Marc O. Rauw. "A SIMULINK environment for Flight Dynamics and Control analysis Application to the DHC-2 Beaver". Master's thesis, Delft University of Technology, Delft, The Netherlands, 1993.

[12] RTCA/SC-159. RTCA/DO-245A: Minimum Aviation System Performance Standards for the Local Area Augmentation System (LAAS). Technical report, RTCA, 2004.

[13] Brian L. Stevens and Frank L. Lewis. *Aircraft Control and Simulation*. Wiley, 1992.